Design of experiments for data-driven optimization in the field of direct metal laser sintering

Dominic Zettel, Piotr Breitkopf, Pascal Nicolay, Roland Willmann

CSMA 2022
15ème Colloque National en Calcul des Structures
16-20 mai 2022, Presqu'île de Giens (Var)

Design of experiments for data-driven optimization in the field of direct metal laser sintering

D. Zettel[1,2] (d.zettel@cuas.at), P. Breitkopf[1] (piotr.breitkopf@utc.fr), P.Nicolay[2] (p.nicolay@cuas.at), R. Willmann[2] (r.willmann@cuas.at),

[1] *UTC, Université de Technologie de Compiègne, France*
[2] *CUAS, Carinthia University of Applied Sciences, Austria*

Abstract — The simulation and modeling of direct metal laser sintering (DMLS) processes are quite challenging due to the complexity and multitude of physical phenomena occurring during the production process. This work investigates how different process parameters (e.g., laser power) influence the correlating material characteristics (e.g., mechanical strength). The ultimate goal of this work is to create a data model which will enable the data-driven multi-optimization of mechanical parts, manufactured by DMLS.
Key words — direct metal laser sintering, data-driven optimization, multi-physical optimization.

1. Introduction

Additive manufacturing (AM), especially laser powder bed fusion (LPBF), is a very complex production technology with a lot of adjustable parameters (e.g., scan speed) [1, p. 1]. An overview of all the single LPBF-parameters is provided by Moges et al. [2, p. 26]. During the printing process, each of these parameters is linked to certain physical phenomena (e.g., fluid dynamics of the molten pool). These physical phenomena often have a mutual influence on each other, affecting the characteristics (e.g., homogeneity) of the printed structure. In the case of standard LPBF-parts, the complexity of the overall manufacturing process is already very high. Indeed, due to a structure's irregular cooling rates depending on its build height and geometry, standard LPBF-parts show an inhomogeneous microstructure with anisotropic material characteristics [3, p. 3]. Furthermore, several influence factors can vary from one print job to the next (e.g., degree of oxidation of powder material) and lead to additional process fluctuations.

The fabrication of parts with given, targeted material characteristics (e.g., mechanical strength, thermal conductivity, vibration damping) requires taking all the physical phenomena, their mutual influence, and their impact on the solidified structure into account. The models mostly take the five following physical phenomena into account: powder layer deposition, delivery of laser energy onto the powder, formation of the melt pool, solidification of the melt pool due to heat dissipation, and development of residual stresses due to different heating and cooling operations. However, the predictive accuracy of these models is strongly affected by modeling assumptions, numerical accuracy, parameter uncertainties, and measurement uncertainties. Furthermore, there is a cascading effect between the different models combined to perform, e.g., multi-scaled simulations, which leads to a further increased inaccuracy in the computed results [2, p. 14]. The geometrical complexity of the structure also affects the computing time for a given model. Higher computing times are often synonymous with poor economic performance [4, pp. 41-42], and even with poor ecological performance, higher energy consumption directly relates to a higher CO2 footprint [5, pp. 46-47].

Another approach is entirely experimental. Here, a series of complementary test samples are thoroughly designed, manufactured, and characterized to quantify the effect of selected process parameters (incl. mutual interaction) on the resulting microstructure, texture, porosity, and mechanical properties (e.g., Young modulus, thermal conductivity, vibration damping) of the printed parts. The

acquired knowledge can then be used, in the Design phase, for multi-physical optimization purposes. It can also be used to help improve existing simulation models.

Therefore, work's overall goal is to develop design guidelines – based on data-driven material studies - that enable the multi-physical optimization of industrial parts fabricated via Direct Metal Laser Sintering (DMLS), as shown in Figure 1.

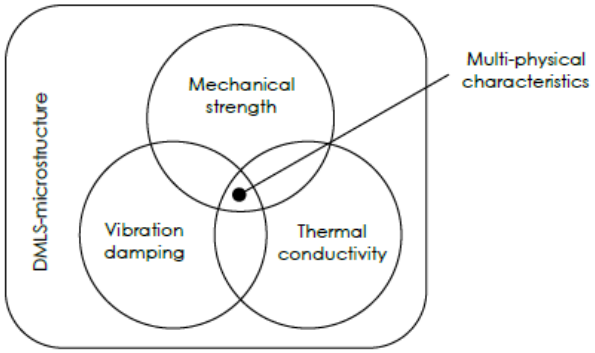

Figure 1: Principle of a multi-physical optimized DMLS-part

1. Method and material

The overall approach to developing and fabricating test specimens with different material characteristics consists of five steps, as schematically shown in Figure 2.

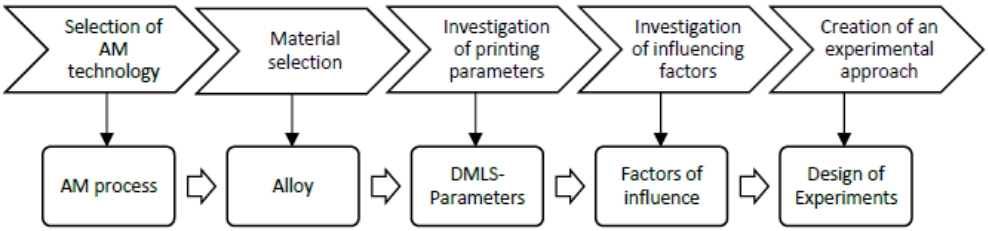

Figure 2: Overall approach regarding the development and fabrication of test specimens with different material characteristics

A suitable AM technology is selected first, with which different material characteristics can be produced using the same base material. Then, the material is selected, considering the needs for subsequent multi-physical optimization tasks, in combination with lightweight design. Next, the relevant process parameters and factors of influence are identified. This approach enables the subsequent design and preparation of the test print jobs, using Design of Experiments (DoE) methods.

1.1 Investigation of printing parameters:

The respective DMLS-parameters, which influence the microstructure of a printed part (e.g., porosity), consist of the laser power, the laser speed, the layer thickness, and hatch distance. The laser power (P) directly correlates to the heat energy used to melt the powder material. The laser speed (v) is the speed of the melt pool. The thickness (t) is the height of the applied powder layers (there might be several of them) before laser exposure. The hatch distance (h) corresponds to the spacing between two neighboring laser paths. The overall energy density (E) can be calculated using these four parameters, as follows:

$$E = \frac{P}{v \cdot h \cdot t} \quad (1)$$

In Table 1, we present the possible range for each parameter (on the EOS M290 printing system), the standard settings for the material that we have selected (i.e., "StrengthAl"), as well the values of the different parameters that we have used in our experiments (DoE).

		Standard settings	DoE		
Parameter	Possible range	"StrengthAl"	Low level	High level	Center point
P [W]	0-370	250	200	300	250
v [mm/s]	0-7000	550	385	715	550
h [mm]	0-x (0.05-0.25)	0,18	0,126	0,234	0,18
t [mm]	steps of 0,03	0,03	0,03	0,09	0,06

Table 1: DMLS process parameters

In the DoE, the laser power changes by ±20%, compared to the standard value. The laser speed changes by ±30%. The layer thickness cannot be changed (it depends on the powder material). However, the number of layers that can be added before exposure can be changed. Therefore, the layer height (t) is a multiple of the thickness of the standard layer. The energy density corresponding to each set of parameters is shown in Figure 3. The colored dots represent parameter sets, with equal energy density.

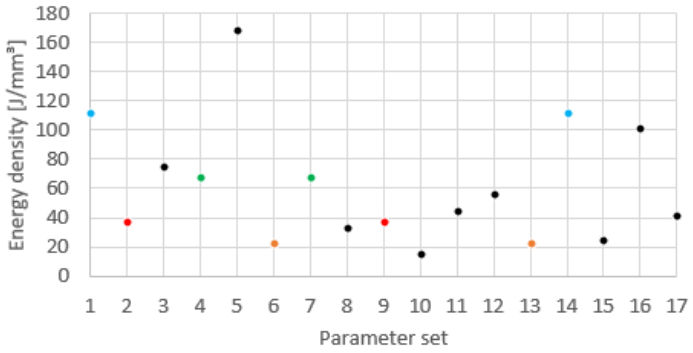

Figure 3: Energy densities, for each specimen

1.2 Experimental method (DoE)

A full factorial design with four factors and two levels was selected. Such a DoE requires 16 experiments. We added one additional experiment (the so-called "center point"). In that case, the printing parameters are simply the average values between the low and high-level settings of the DoE. Five probes were also printed (test prints) to help assess process issues beforehand. The probes are rectangular solids, with a surface of 10x10mm and a height of 0,5mm (marking not included). In the case of high-energy inputs, they are necessary to check whether the structure (or rather, the powder material) will be "burned" or not. In case of low energy inputs, they are necessary to check whether the powder material will still be melted or not.

The print jobs were printed using an EOS M290 system. This system comes with a platform of 250x250x325mm^3 (made of Alumina 3.3547) and a 400W Yb-fiber laser. The standard spot size is 100μm (however, the spot size depends on the applied Laser power). The atmosphere in the printing chamber consists of Argon with a maximum oxygen content of 0.1%. Every layer of the print job is

documented via EOSTATE, a software solution by EOS GmbH that takes a picture before every recoating and exposure operation.

The printing platform was divided into nine sections (grid “a”-“i”), as shown in Figure 4. Each of the 17 test specimens (experiments) was printed repeatedly in each of the five highlighted sections. This segmentation and reproduction of the same test specimen at different locations enable the subsequent investigation and consideration of possible process variations, mainly due to variations of the laser focal point and incident angle all over the platform. The test specimens are cylinders with a height of 103mm and a diameter of 8mm. The specimens are directly printed onto the platform without a support structure.

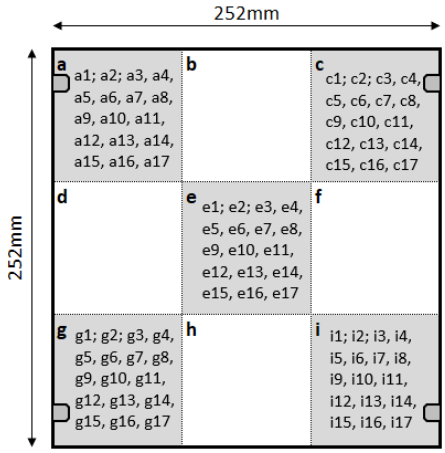

Figure 4: Build platform grid

The first and second print jobs crashed at a “build height” of 45.25mm (i.e., 1509 layers) and 59.94mm (i.e., 1984 layers), respectively, although the test structures were perfectly printed. These failures were probably due to heat dissipation issues, which became increasingly important as the height of the samples increased (the higher they are, the more difficult it becomes to dissipate the stored energy). This behavior leads to internal stresses that force the specimens to bend. The bending causes issues in the powder repartition, with unwished consequences. Fortunately, the specimens of the second print job reached a sufficient height to be exploited. The platform (and attached specimens) was unpacked and put in a hardening oven at the end of the printing operation. The specimens were held for 6 hours at a temperature of 360°C, followed by slow cooling in air. Then, the specimens were further processed on a turning machine to achieve the required test geometries. Three different test specimens, as obtained after this last operation, are shown in Figure 5. Differences in pore sizes are clearly visible.

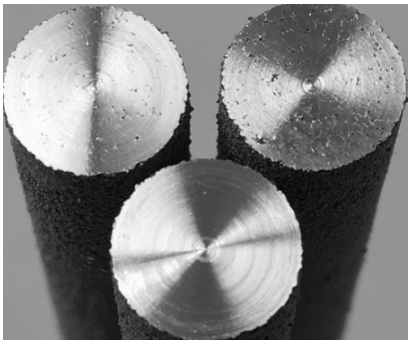
Figure 5: Printed specimens, with different parameter sets. Differences in the pore sizes are clearly visible.

2. Material characterization results

2.1 Mechanical strength

The testing of the mechanical characteristics of the printed specimens was executed on a "Zwick Roell Z020 AlroundLine" tensile testing machine. Therefore, the test geometry of the specimens was defined according to the DIN 50125:2016-12 standard (Form B). The tensile tests themselves were executed according to the ISO 6892-1:2019 standard (Method A). Two sets of specimens (i.e., 2x17 specimens: grid "a" and grid "I," see Figure 4) were tested. The tensile tests were performed at room temperature (22°C). The measurement results are shown in Figure 6.

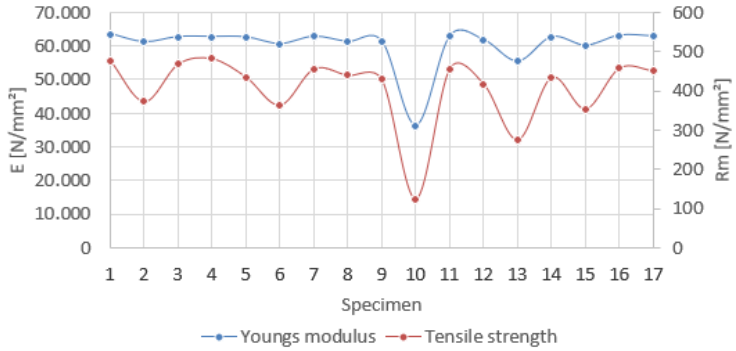

Figure 6: Tensile test results, for the 2x17 specimens, of grid "a" and grid "i".

Figure 6 shows a correlation between tensile strength (Rm) and Young modulus (E). The comparison between samples 6 and 13, which have the same energy density (see Table 2) but show different values of Rm and E, also demonstrates that the energy density does not account for the observed properties alone.

Specimen	P [W]	v [mm/s]	h [mm]	t [mm]	E [J/mm³]
6	300	687,5	0,216	0,09	22,45
13	200	687,5	0,144	0,09	22,45

Table 2: Parameter sets 6 and 13 of DoE

2.2 Temperature gradient

Two sets of specimens (2x17 specimens: grid "e" and grid "g") were tested using a self-designed setup. This setup essentially consists of a hot plate (50°C) and a cold plate (0°C), brought into contact with both ends of the specimens using heat-conducting paste. A specific mounting procedure was designed to ensure the reproducibility of the measurement results, and the comparison between the measurement results obtained for the different specimens. Particular care was taken when applying the glue to ensure a constant thickness. The temperatures are measured using PT1000 sensors, located precisely at the two physical ends of the specimens (see Figure 7). First, we performed measurements of the observed temperature gradients, between both PT1000 sensors, at thermal equilibrium. The measurement results are shown in Figure 8. Discrepancies are again observed between the different specimens.

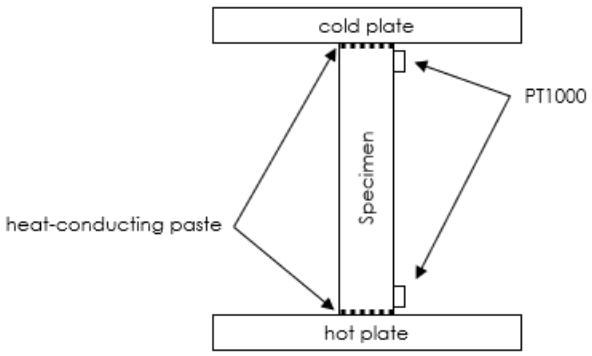

Figure 7: Schematics of the self-made test setup, for temperature gradient measurements

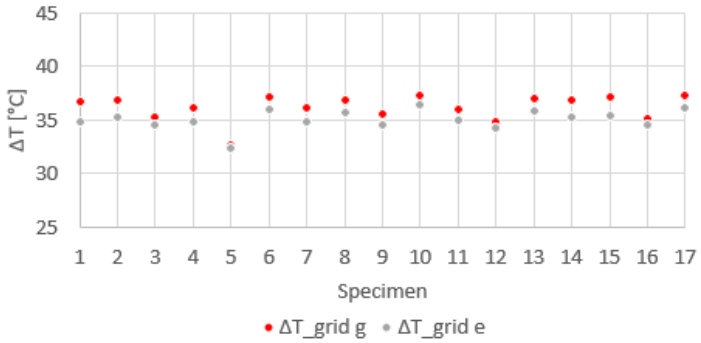

Figure 8: Observed temperature gradients, for the 2x17 specimens of grid “e” and grid “g”

In that case, there is a good correlation between energy density and observed gradient. A higher energy density corresponds to a low gradient, whereas a lower density corresponds to a higher gradient. This correlation was expected due to the growing porosity when the energy density is reduced.

3. Conclusion

This work presented the first characterization results (i.e., tensile strength and temperature gradient in one specific configuration) of 17 different specimens, which were printed using an EOS M290 metal 3D printer. Each specimen was printed using a different set of printing parameters (laser power, laser speed, hatch distance, and layer thickness) to evaluate the effect of each of these parameters on the mechanical and thermal properties of the manufactured specimens.

The tensile test results show a clear correlation between tensile strength and Young’s modulus. The results also show that the energy density alone is not enough to account for the observed variations (in the material properties), from one specimen to the other. A detailed understanding of the results obtained requires a detailed investigation of the effect of the different parameters on the microstructure and texture (incl. porosity) of the samples produced. Future work includes scanning electron microscopy (SEM) and energy dispersive x-ray (EDX) analyses, whose outcomes should allow us to interpret better the preliminary results presented in this paper.

References

[1] J. Oliveira, A. LaLonde, J. Ma, "Processing parameters in laser powder bed fusion metal additive manufacturing," Materials & Design (193); ISSN 0264-1275, pp. 1-12, 2020.

[2] T. Moges, G. Ameta, P. Witherell, „A Review of Model Inaccuracy and Parameter Uncertainty in Laser Powder Bed Fusion Models and Simulations“ Journal of Manufacturing Science and Engineering 141 (4), ISSN 1087-1357, pp. 1-14, 2019.

[3] Z. Çağatay Öter, "www.researchgate.net," September 2017. [Online]. Available: https://www.researchgate.net/publication/320034353_Anisotropic_Mechanical_Behavior_of_Direct_Metal_Laser_Sintering_DMLS_Parts. [Accessed 02 July 2021].

[4] The Minerals, Metals & Materials Society (TMS), "Modeling Across Scales: A Roadmapping Study for Connecting Materials Models and Simulations Across Length and Time Scales," The Minerals, Metals & Materials Society (TMS), ISBN 9780692376065, Warrendale, PA 15086, 2015.

[5] B. Saha, "Green Computing," International Journal of Computer Trends and Technology (IJCTT), volume 14 number 2, ISSN 2231-2803, pp. 46-50, 2014.